#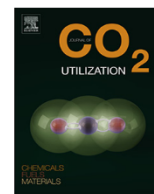 Carbonation of the synthetic calcium silicate hydrate (C-S-H) under different concentrations of CO2: Chemical phases analysis and kinetics

N.B. When citing this work, cite the original published paper.

(article starts on next page)

ELSEVIER

Carbonation of the synthetic calcium silicate hydrate (C-S-H) under different concentrations of CO$_2$: Chemical phases analysis and kinetics

Yongqiang Li[a,b], Wei Liu[b,*], Feng Xing[a,b], Shuping Wang[c], Luping Tang[d], Shifa Lin[b], Zhijun Dong[e]

[a] Institute of Engineering Mechanics, China Earthquake Administration, Key Laboratory of Earthquake Engineering and Engineering Vibration, China Earthquake Administration, 150000, Heilongjiang, China
[b] Guangdong Provincial Key Laboratory of Durability for Marine Civil Engineering, Shenzhen Durability Centre for Civil Engineering, College of Civil and Transportation Engineering, Shenzhen University, Shenzhen, 518060, Guangdong, China
[c] College of Materials Science and Engineering, Chongqing University, 400045, Chongqing, China
[d] Division of Building Technology, Chalmers University of Technology, 41296, Gothenburg, Sweden
[e] Institute of Technology for Marine Civil Engineering, Shenzhen Institute of Information Technology, Shenzhen, 518172, Guangdong, China

A B S T R A C T

In this study, the chemical phases analysis and the kinetics of synthetic calcium silicate hydrate (C-S-H) under differentCO$_2$concentrations (natural (0.03%), 3%, 10%, 20%, 50%, 100%) were investigated. For this aim, the scanning electron microscope (SEM) and transmission electron microscope (TEM) were employed for microstructure characterisation. The ^{29}Si magic angle spinning nuclear magnetic resonance (^{29}Si MAS NMR), X-ray diffraction (XRD) and thermogravimetric analysis (TGA) coupled with mass spectrometer (MS) were used for characterising the chemical phases before and after carbonation. From the NMR results, it was found that C-S-H would be partly decalcified under the natural condition but completely under the accelerated conditions. Two equations related to the carbonation kinetics under natural and accelerated conditions were proposed respectively. The compositions in decalcified C-S-H were not affected by the CO$_2$ concentration. The XRD analysis showed that vaterite, aragonite and calcite were coexistent after carbonation, which would be transformed to aragonite and calcite with further carbonation. The preferential formation of the allotropic calcium carbonate was not impacted by the concentration of CO$_2$ either. Based on the TGA-MS test, the stoichiometric formula of synthetic C-S-H was determined with $CaO \cdot SiO_2 \cdot 0.87H_2O$ or $C \cdot S \cdot H_{0.87}$. In addition, a carbonation kinetics model was proposed to learn the carbonation kinetics of C-S-H carbonated in different CO$_2$ concentrations. The experimental data fitted well with the model. The carbonation kinetics between 3% and 20% CO$_2$ are similar, but different from that under 50% and 100% CO$_2$.

1. Introduction

Almost all of the concrete structures have to undergo the carbonation reaction, because of the abundant sources of CO$_2$ in atmosphere, which will then decrease the pH value of pore solution inside concrete, and finally cause the depassivation of steel reinforcement, resulting in the reduced working lifetime of concrete structure eventually [1,2]. Due to the widespread and high potential of concrete to become the most efficient agent to capture the CO$_2$, the CO$_2$ storage capacity of concrete becomes a hot topic recently [3].

The calcium-silicate-hydrate (C-S-H), which is the most influential hydration product for the final strength of concrete, is vulnerable to carbonation [4,5]. It is also the main component in concrete to absorb and store the atmospheric CO$_2$. However, C-S-H in concrete is blended with other hydration products, and presents as amorphous and inhomogeneous phases in concrete—all of which made the performance of this product difficult to be studied, especially that the carbonation of pure C-S-H is not clear. For instance, Morandeau et al. [6] has studied the carbonation mechanism of C-S-H through the carbonation of cement paste and mortar, but their results still cannot explain the chemical phases' transformation of pure C-S-H during carbonation. It is therefore more reasonable to study the carbonation performance of pure C-S-H through laboratory experiments by using the synthetic C-S-H [7–10]. Similar research has been done by Sevelsted et al. [4] to evaluate the carbonation performance of C-S-H with varying Ca/Si ratio, but their results are only suitable for the atmospheric carbonation and the allotropic precipitation of calcium carbonate after carbonation is absent in their results.

---

* Corresponding author.
  E-mail address: liuwei@szu.edu.cn (W. Liu).

According to the model proposed by Taylor [11,12], the 1.4 nm tobermorite can be used to describe the C-S-H structure with lower Ca/Si ratio while jennite is more suitable for representing C-S-H with higher Ca/Si. For the C-S-H hydrated from C$_3$S or OPC cement, the Ca/Si ratio are varying from 1.2 to 2.1 with an average value of 1.75 [13]. To understand the carbonation behaviour of pure C-S-H in cement paste, Morales-Florez et al. [14] have chemically synthesized the C-S-H with Ca/Si = 1.8 which is close to the average ratio in Portland cement paste. However, when supplementary cement materials (SCM), such as silica fume, fly ash or slag, are used to replace Portland cement [15], the mean value of C-S-H in the hydrated mixture will be decreased to approximately 1 [16,17]. In such condition, the tobermorite-like model should be better to describe C-S-H structure. The Ca/Si ratio of tobermorite varies between 1 and 1.5 with different degrees of protonation. If all of the bridging silicate tetrahedra are protonated the Ca/Si should equal to 1 [13], which is closer to the value for the SCM mixed cement paste. Therefore, it is necessary to investigate the carbonation performance of C-S-H in cement paste with SCM by synthetic C-S-H with Ca/Si ratio of 1. Besides, Sevelsted et al. [4] suggested that C-S-H with Ca/Si higher than 0.67 will be decalcified to Ca/Si = 0.67 first and then decomposed to form calcium carbonate and calcium modified silica gel under the effect of carbonation. While some researches have studied the carbonation performance of C-S-H with different Ca/Si ratios under the atmospheric environment [4,18], the results from this paper can be the representative for characterizing the carbonation performance of C-S-H with Ca/Si > 0.67 under accelerated carbonation.

An observation of the C-S-H structure clearly indicates that calcium is covalently connected to the silicon chain via oxygen atoms, but balanced with Ca^{2+} from the pore solution. When C-S-H is carbonated, calcium would be decalcified to precipitate as calcium carbonate, with the formation of calcium modified silica gel, causing higher polymerisation of C-S-H [4,19–21]. Three allotropic kinds of calcium carbonate, named as calcite, vaterite and aragonite, are usually formed in the carbonated C-S-H [22–24]. The formation of amorphous calcium carbonate is also investigated and reported by some researchers [6,25]. There are several reasons, including difference in supersaturation [26], pH [27], surface of nucleation [28], temperature, humidity and CO$_2$ concentration [1,29], that may affect the polymorphic precipitation of calcium carbonate. However, until now, they are no obvious nor simple explanation for this preferential polymorphic precipitation [30].

The concrete carbonation rate are controlled by several reasons such as temperature, humidity and CO$_2$ concentration. It is reported that carbonation rate reached maximum within the range of 50–70% RH [29]. Drouet et al. [31] found that, for CEM I the carbonation rate increased linearly within the temperature ranging from 20 to 80 °C, whilst

for CEM V, it increased between 20 and 50 °C but decreased between 50 and 80 °C. Cui et al. [32] suggested that carbonation depth was increased with increasing CO$_2$ concentration but its effect is reduced when CO$_2$ concentration beyond 20%. In this study, however, only the effect of CO$_2$ concentration was considered. Actually, the carbonation rate under natural condition is too slow to be applied for extensive research. Usually, the accelerated carbonation with high CO$_2$ concentration is widely used in laboratories to give an evaluation of carbonation resistance of cement-based materials. However, the recommended CO$_2$ concentration for accelerated carbonation experiments varies from countries. For instance, it is recommended by governments to use 1%, 2%, 3% and 4% CO$_2$ in Belgium, Germany, some Nordic countries and UK respectively [30,33], while 20% CO$_2$ is required in China [34]. A uniform standard applying for accelerated carbonation has not been reached until now, while much higher CO$_2$ concentration, such as 50% or 100%, are even used by some researchers in laboratory experiments [32,35,36].

In the present work, the C-S-H with 1.0 Ca/Si molar ratio was used for both natural (0.03% CO$_2$ concentration) and accelerated carbonation (3%, 10%, 20%, 50% and 100% CO$_2$ concentration). The microstructure characterisations of the C-S-H samples were investigated by the aid of scanning electron microscope (SEM) and transmission electron microscope (TEM). Furthermore, to present qualitative and quantitative analysis of the Si configuration inside C-S-H after carbonation, the ^{29}Si magic angle spinning nuclear magnetic resonance (^{29}Si MAS NMR) measurement was employed. Relative proportion of allotropic calcium carbonate was measured via X-ray diffraction (XRD). The theoretical analysis of the carbonation kinetics of the synthetic C-S-H under different CO$_2$ concentrations have been studied in detail. The results from this investigation also contribute to the CO$_2$ storage by cementitious materials and the carbonation of recycled concrete.

2. Materials and methods

2.1. Synthesis of calcium silicate hydrate

Hydrothermal synthesis method was applied to produce the amorphous calcium silicate hydrate (C-S-H) by mixing the slurry of lime and amorphous SiO$_2$ in an autoclave. The Ca/Si molar ratio of initial material was 1:1 and water solid ratio in mass was 10:1. It was synthesised at the temperature of 120 °C for 7 h with a stirring speed of 400 rpm, followed by filtering and oven-drying at 80 °C. The chosen way for the C-S-H synthesis (120 °C) probably conducts to better crystallization compared to C-S-H in the field. More details of C-S-H synthesis were described in another study [37]. Finally, the powder shape of pure C-S-H with irregular appearance was collected as shown in Fig. 1(a). The
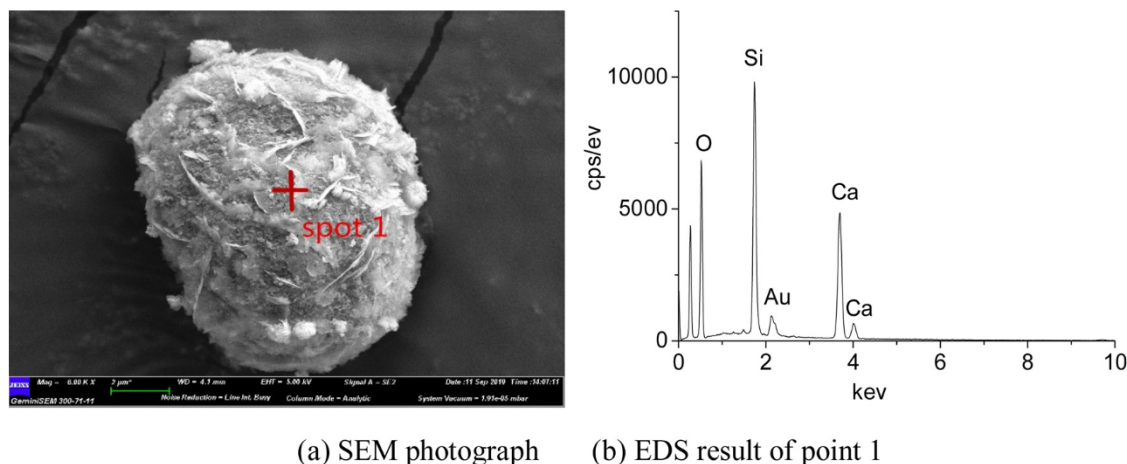

(a) SEM photograph   (b) EDS result of point 1

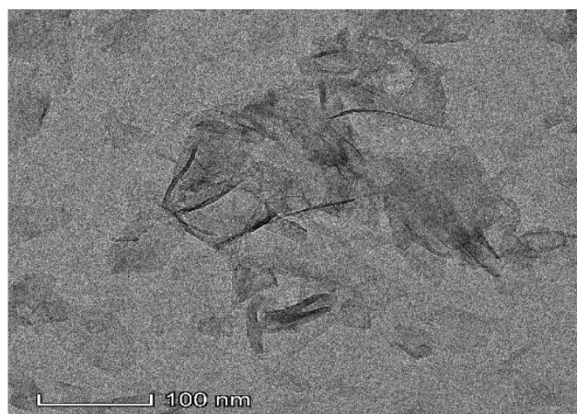**Fig. 1.** SEM photograph and EDS result of the synthetic C-S-H.
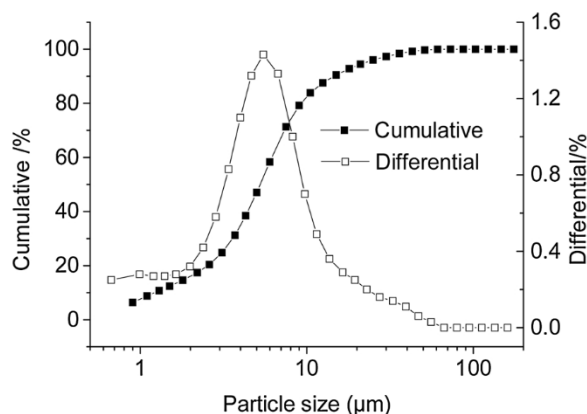
Fig. 2. TEM image of the synthetic C-S-H.

Fig. 3. Particle distribution of synthetic C-S-H.

energy dispersive spectrometer (EDS) analysis in Fig. 1(b) verifies the high intensity of Ca, Si and O, and gives the atomic ratio of Ca/Si = 1.0. Also, Fig. 2 gives the nano-structure of synthetic C-S-H from TEM observation, showing the compositions of foil sheets. Particle size of C-S-H powder is obtained using a laser particle analyser as presented in Fig. 3. The values of the measured mean particle size D [4,3] is 7.21 μm. The uncarbonated sample was labelled as reference in this study.

2.2. Accelerated carbonation

The synthetic C-S-H powder samples with three grams weight were loosely dispersed on the bottom of an aluminium container with a diameter of 55 mm. For the natural carbonation, the sample containers were placed in a climate environment with a mean temperature of 25 °C and a relative humidity ranging from 40% to 75%. The CO_2 concentration in the climate of the room was approximately 0.03% [1]. For the accelerated carbonation, as displayed in Fig. 4, the sample
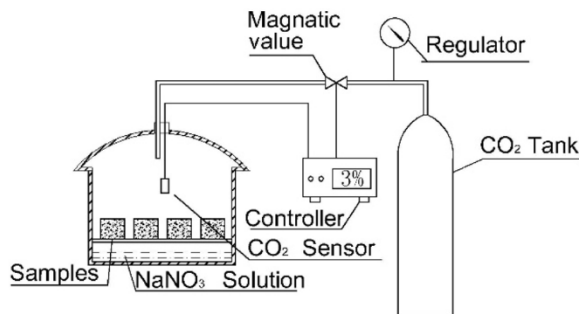

Fig. 4. Sketch of carbonation device.

containers were put into the newly designed carbonation chambers. More details of the accelerated carbonation chamber were described in another study [38]. The relative humidity and temperature for the accelerated carbonation were maintained at 72 ± 2% and 20 ± 2 °C, respectively. Different concentrations of CO_2 (3%, 10%, 20%, 50% and 100%) were applied with 0.5% fluctuation. Because only the difference of CO_2 concentration was considered in this study, the effect of slight difference in temperature and humidity between the natural and accelerated carbonations was ignored. The mass changes of all the samples were measured during the whole carbonation process, which showed that the mass became stable after 20 days, indicating a completion of carbonation at that time. The NMR measurements were, therefore, applied after carbonating for 20 days. The sample carbonated at 100% CO_2 was also measured after 60 days of carbonation to investigate the effect of exposure time on the decalcification process. The XRD measurements were carried out after carbonation for 20 and 60 days, respectively.

2.3. Microstructure characterisation

2.3.1. ²⁹Si MAS NMR
To detect the silicate configuration transformation of synthetic C-S-H after carbonation, ²⁹Si MAS NMR measurements were carried out in a JEOL ECZ600MHz (14.1 T) spectrometer. Samples were packed in 8 mm ZrO_2 rotors to spin at the speed of 5 kHz and $\Upsilon B/2\pi = 40$ kHz, whilst parameters for relaxation delay and scanning numbers were determined as 60 s and 512 times respectively. The chemical shifts were referenced to trimethylsilyl (TSPA)

2.3.2. XRD analysis
To identify the mineral compositions before and after carbonation, C-S-H samples without pre-drying were measured by XRD powder diffractometer (Bruker, D8 Advance) with Cu K_α radiation at 40 kV and 40 mA. Measuring range was set as 5–70° 2θ with 0.02° step and 1 s step time. Qualitative analysis of chemical phases was finished in EVA software and quantitative analysis of the relative content of calcium carbonate was given via TOPAS software.

2.3.3. Thermal analysis
The thermogravimetric analysis (TGA) tests were performed at Netzsch STA 449 F5 under N_2 atmosphere coupled with a mass spectrometer (MS) Netzsch QMS 403D Quadrupole. The sample without carbonation (14.3 mg) was heated under a nitrogen atmosphere (250 ml/min) in a corundum crucible varying from 30 °C to 1000 °C, with the heating rate of 10 °C/min.

2.3.4. SEM and TEM
The microstructure was observed by ZEISS Gemini SEM and its nano-structure was further characterised by FEI Talos 2000 TEM. Before the SEM observation, the powder samples were scattered uniformly on the surface of a conductive film and then coated with the thin gold, and ultrasonic dispersion technique was used to disperse samples immersed in ethanol before the TEM test.

3. Results

3.1. ²⁹Si MAS NMR results

The ²⁹Si MAS NMR spectra of synthetic C-S-H before and after carbonation under different CO_2 concentrations were demonstrated in Fig. 5. All of the spectra were deconvolved into several peaks with different polymerization degrees(Q_n, n = 0, 1, 2, 3, 4), representing the connectivity of Si atoms [39], to give quantitative information of Si coordination with fitting accuracy kept at $R^2 \geq 0.98$. The isolated tetrahedra Q_0 was not detected for any of the samples, as a result of the absence of C_3S and C_2S [20,30].
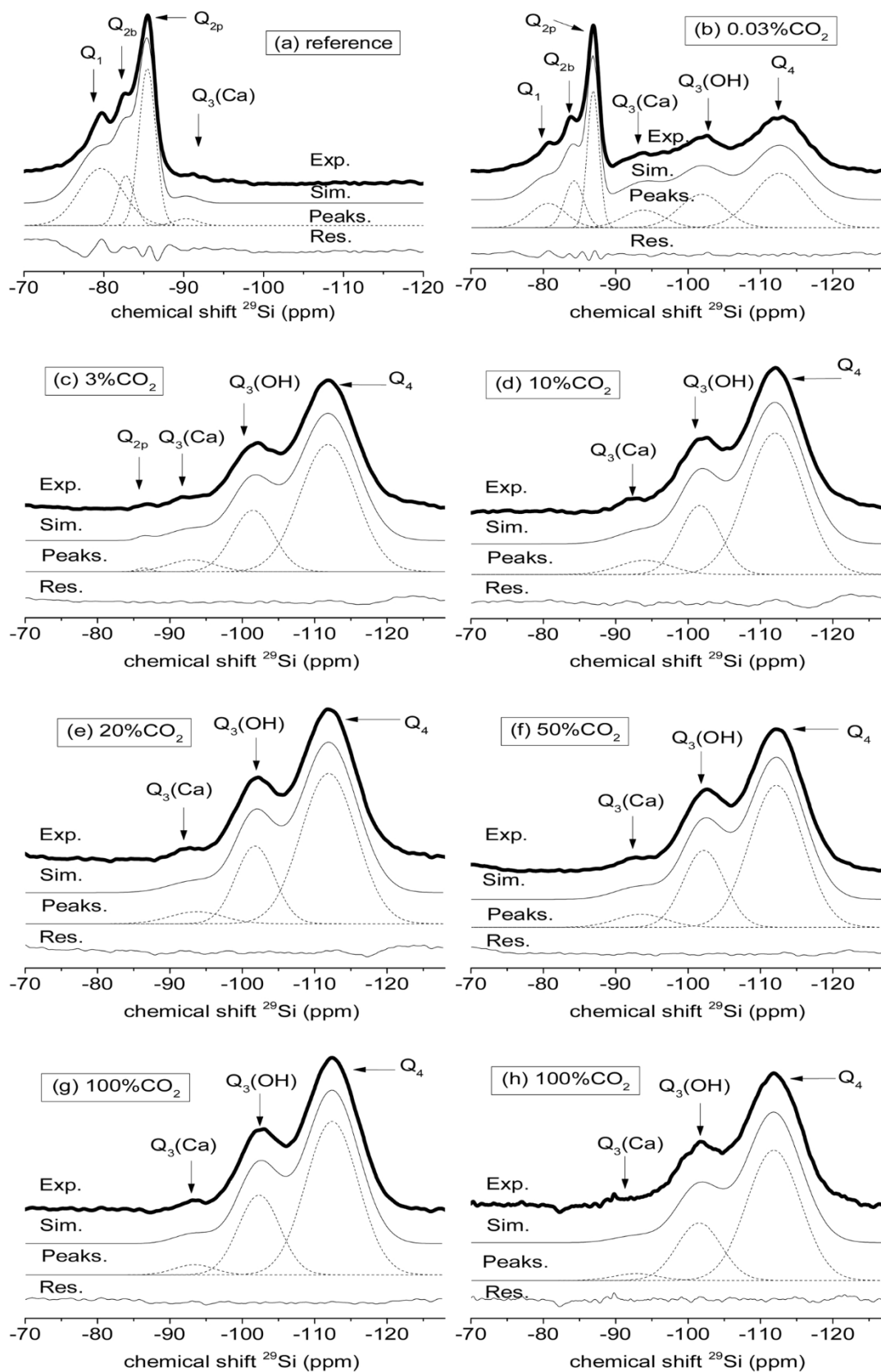
Fig. 5. ^{29}Si MAS NMR spectra of C-S-H gel after carbonation of 20 days (a)-(g) and 60 days (h) (Exp. = experimental result, Sim. = simulated spectra, Peak. = separating simulated peaks, Res. = difference between experimental and simulated result, the fitting accuracy was controlled at $R^2 \geq 0.98$).

For the reference sample which was uncarbonated, four distinct peaks were deconvolved, i.e. the end groups or dimers (Q_1, -79.6 ppm), the bridging sites (Q_{2b}, - 82.8 ppm) and paired sites (Q_{2p}, -85.4 ppm), and only traceable content of high polymerised chain Q_3(Ca), locating at -90.3 ppm ($(SiO-)_3Si^*-1/2Ca$), which was in agreement with the previous studies [8,9,40–44]. It is noteworthy that the deconvolution results of this pure C-S-H were different from that of the cement paste: two peaks of Q_2 (Q_{2b} and Q_{2p}) were deconvolved from the spectrum, while only one peak of Q_2 was found in the cement paste sample with high Ca/ Si ratio [38], which is also consistent with the results shown in [4].

After carbonation, Q_1 and Q_2 were almost disappeared with the increase of Q_3(Ca) (locating from -92.8 to -93.9 ppm), and at the same time, other silica rich phases were formed. The peak shifts assigned from -101.2 to -102.3 ppm were a representative of hydroxylated Si tetrahedrons (Q_3(OH), $(SiO)_3-Si-OH$), while peaks from -111.8 to -112.7 ppm were attributed to the formation of Q_4 where all of the calcium atoms were decalcified and silicate tetrahedrons were condensed as quartz-like silica gel [29,45].

The deconvolution results for the chemical shift and proportion of Q_n were listed in Table 1. For the reference sample, the main composition was C-S-H with relatively low connectivity, because Q_1 (41%), Q_{2b} (13%) and Q_{2p} (43%) were the major proportions, and only 3% Q_3 was found in the structure, causing by the natural carbonation during sample preparation. When natural carbonation (0.03% CO_2) was considered, the proportions of Q_1 and Q_2 were dramatically decreased, while quite amount of calcium-modified silica gel including Q_3(Ca), Q_3(OH) and Q_4 appeared after carbonation. However, only part of C-S-H was carbonated at the atmospheric environment (0.03% CO_2) since certain proportions of Q_1 and Q_2 were still remained. This result was consistent with the former study that C-S-H was difficult to be fully carbonated in the natural condition [20,30]. The mean chain length of SiO_4 $\bar{CL}$ tetrahedra can thus be calculated with Eq. (1) [4], where $I(Q^n)$ represents the content of Q_n (%). Here only values of the sample before and after natural carbonation were given, because the samples after the accelerated carbonations were completely decalcified without the remaining of C-S-H related peaks (Q_1, Q_{2b} and Q_{2p}). Table 1 shows that $\bar{CL}$ was significantly lengthened from 4.7 to 7.8 after natural carbonation, which was caused by the polymerization of Si tetrahedra.

$$\bar{CL} = 2[I(Q_1) + I(Q_{2b}) + I(Q_{2p})]/I(Q_1) \tag{1}$$

When samples were carbonated at accelerated conditions from 3% to 100% CO_2, totally different results were found compared to that under natural condition. In the view of Table 1, Q_1, Q_{2b} and Q_{2p} were entirely vanished under the accelerated carbonation, except for the sample that was kept at 3% CO_2, which still had 1% Q_{2b} left. The proportions of Q_3(Ca), Q_3(OH) and Q_4 in carbonated phases were approximately 5%, 25% and 70%, respectively. All of the C-S-H samples were carbonated to stay as decalcified C-S-H (including calcium modified silica gel and silica gel) and calcium carbonate.

Further comparison was made between the samples carbonated under 100% CO_2. When the carbonation period increased from 20 days to 60 days, the proportion of Q_3(OH) was slightly decreased (by 2%),

accompanying with a small increase of Q_4 (by 2%). This indicates a higher polymerisation after a longer carbonation duration. However, this polymerisation process seems to be very slow. By using Eq. (2) below, the level of decalcification, L_d, could be evaluated, as displayed in Table 3 [30]:

$$L_d = \left(1 - \frac{Q_1^a + Q_{2b}^a + Q_{2p}^a}{Q_1^b + Q_{2b}^b + Q_{2p}^b}\right) \times 100\% \tag{2}$$

where Q_1^a, Q_{2b}^a, and Q_{2p}^a represent the proportions of Q_1, Q_{2b} and Q_{2p} after carbonation, respectively, while Q_1^b, Q_{2b}^b, Q_{2p}^b indicate those in the sample before carbonation.

The decalcification level L_d, as shown in Table 2, has reached almost 100% for all the samples under the accelerated conditions, verifying the fact that C-S-H has been completely decalcified, while it was only 59.5% for the one under the natural carbonation (0.03% CO_2). In addition, what should be emphasised from Table 2 is that the values of $Q_4/(Q_3(Ca) + Q_3(OH))$ under all the accelerated conditions are between 2.0 and 2.5 with average value of 2.3, suggesting the similar compositions in decalcified C-S-H.

Mass change shows that there is no further mass increase even for natural carbonation after 20 days, indicating the completion of the carbonation process in 20 days. Hence, it can be concluded that carbonation of C-S-H under natural condition and accelerated conditions are different: only a portion of C-S-H will be decalcified under natural condition, while under accelerated conditions all of the C-S-H will be decalcified. CO_2 concentration will not affect the compositions of decalcified C-S-H (including calcium modified silica gel and silica gel). Besides, when the duration time of carbonation is prolonged, the degree of polymerisation will be improved further.

3.2. XRD results

The XRD spectra of synthetic C-S-H before and after carbonation are presented in Fig. 6. For the reference sample, diffused peaks instead of sharps peaks were presented at 2θ of 29.4°, 32° and 50° in the spectra, indicating the appearance of amorphous C-S-H. After carbonation under ambient condition (0.03% CO_2), the peaks at 2θ of 32° and 50° were disappeared, meanwhile the peak at 2θ of 29.4° was narrowed and its intensity was decreased. Different types of calcium carbonate formed with the appearance of calcite, aragonite and vaterite. Vaterite became the dominant phase after accelerated carbonation.

Despite that the peak at 2θ of 29.4° is characteristic for both C-S-H and calcite, NMR results above at the Section 3.1 demonstrated that the C-S-H was completely decalcified under accelerated carbonation, so that the peak located at 29.4° could be considered as the existence of calcite. The content of C-S-H therefore was not considered in the quantitative analysis. As a result, the relative proportion of the crystalline forms of carbonated products can be quantitatively analysed by Rietveld refinement. Results are displayed in Tables 3 and 4. It showed that vaterite was the dominate phase under all the carbonation conditions conducted in this study, which contains approximately 92% content of all the detectable mineral compositions. For calcite, the

Table 1
Deconvolution results of ^{29}Si MAS NMR spectrum of the samples before and after carbonation (%).

ppm from TSPA (I(Qₙ) (%))	Carbonation time (d)	Q_1	Q_{2b}	Q_{2p}	Q_3(Ca)	Q_3(OH)	Q_4	$\bar{CL}$
Reference	20	−79.6 (41)	−82.8 (13)	−85.4 (43)	−90.3 (3)	−	−	4.7
Natural (0.03% CO_2)	20	−80.7 (10)	−84.3 (10)	−86.9 (19)	−93.9 (8)	−101.9 (18)	−112.7 (35)	7.8
3% CO_2	20	−	−	−86.4 (1)	−93 (5)	−101.5 (25)	−111.9 (69)	−
10% CO_2	20	−	−	−	−93.9 (6)	−101.7 (24)	−112 (70)	−
20% CO_2	20	−	−	−	−93.7 (5)	−101.8 (25)	−111.9 (70)	−
50% CO_2	20	−	−	−	−93.5 (6)	−101.2 (27)	−112.2 (67)	−
100% CO_2	20	−	−	−	−93.4 (3)	−102.3 (28)	−112.4 (69)	−
100% CO_2	60	−	−	−	−92.8 (3)	−101.5 (26)	−111.8 (71)	−

Table 2
Decalcification of the C-S-H induced by carbonation calculated from ^{29}Si NMR and Eq. (2).

Sample	Carbonation time (d)	$Q_1 + Q_{2b} + Q_{2p}$ (%)	L_d (%)	$Q_3(Ca) + Q_3(OH) + Q_4$(%)	$Q_4/(Q_3(Ca) + Q_3(OH))$ (%)
Reference	20	97	0	3	0.0
Natural (0.03% CO₂)	20	39	60	61	1.3
3% CO₂	20	1	99	99	2.3
10% CO₂	20	0	100	100	2.3
20% CO₂	20	0	100	100	2.3
50% CO₂	20	0	100	100	2.0
100% CO₂	20	0	100	100	2.2
100% CO₂	60	0	100	100	2.4

amount varied from 3.3% to 4% under the accelerated conditions, but increased to 7.1% under the natural carbonation (0.03% CO₂). A slight amount of aragonite was formed after carbonation. Because of the quite similar content of vaterite, aragonite and calcite, it can be assumed that the preferential precipitation of polymorphic calcium carbonate is independent of the CO₂ concentration.

In the view of the relative proportion of carbonated phases between 20 and 60 days, there was a decrease in the amount of vaterite and an increase of another two polymorphic calcium carbonate, i.e. aragonite and calcite, were observed. This finding indicated that the phase transformation from vaterite to aragonite and calcite occured during carbonation reaction, even when the decalcification process was completed. Pretty low rate of transformation speed (lower than 1% between 20 and 60 days under the accelerated conditions) was also verified when the carbonation was finished after 20 days, as demonstrated in [28,30,46,47]. The vaterite and aragonite—the thermodynamically unstable forms—are expected to transform into calcite as a final state after long time curing.

3.3. Carbonation kinetics of C-S-H under different CO₂ concentrations

3.3.1. Stoichiometric formula of synthetic C-S-H

The reference sample without carbonation was selected to measure with TGA-MS, as shown in Fig. 7, to determine the stoichiometric formula of synthetic C-S-H. According to the TGA-MS results, 11.83% mass loss was detected at the temperature between 105 °C and 818 °C, which was attributed to the C-S-H dehydration. No obvious emission of CO₂ was detected, suggesting the high purity of produced C-S-H. The exothermic peak at 833.2 °C indicated a phase transformation to wollastonite [48].
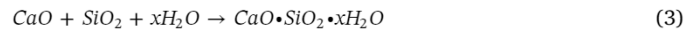
If mass balance was considered, when CaO and SiO₂ were mixed with initial Ca/Si = 1.0, 1 mol of $CaO \cdot SiO_2 \cdot xH_2O$ would be synthesized (Eq. (3)). Therefore, the mass loss from the dehydration of C-S-H (W_1) can be expressed in Eq. (4). For the totally carbonated C-S-H, the carbonation reaction should follow the Eq. (5), and the ideal maximum mass increase W_{max} can be calculated by Eq. (6).

Table 3
Rietveld refinement results of carbonated C-S-H under different CO₂ concentrations after 20 days.

Sample	Vaterite	Aragonite	Calcite	Others
0.03%CO₂	91.3	0.9	7.1	0.7
3% CO₂	92.3	1.1	3.8	2.8
10 %CO₂	92.6	1.5	3.3	2.6
20% CO₂	92.5	0.7	3.9	2.9
50% CO₂	92.1	0.8	4.0	3.1
100% CO₂	91.5	1.2	3.8	3.5

Table 4
Rietveld refinement results of carbonated C-S-H under different CO₂ concentrations after 60 days.

Sample	Vaterite	Aragonite	Calcite	Others
0.03%CO₂	87.8	0.7	9.4	2.1
3% CO₂	91.4	1.9	3.5	3.2
10 %CO₂	91.1	1.9	3.7	3.3
20% CO₂	91.9	1.7	3.5	2.9
50% CO₂	92.1	1.9	4.1	1.9
100% CO₂	91.2	1.6	4.1	3.1

$$CaO + SiO_2 + xH_2O \rightarrow CaO \cdot SiO_2 \cdot xH_2O \qquad (3)$$

$$W_1 = \frac{18.01x}{56.08 + 60.08 + 18.01x} \times 100\% \qquad (4)$$

$$CaO \cdot SiO_2 \cdot xH_2O + CO_2 \rightarrow CaCO_3 + SiO_2 \cdot xH_2O \qquad (5)$$

$$W_{max} = \frac{44.01}{56.08 + 60.08 + 18.01x + 44.01} \times 100\% \qquad (6)$$

Based on the mass loss value from the TGA spectrum, and Eq. (4), the stoichiometric formula of synthetic C-S-H could be determined with $CaO \cdot SiO_2 \cdot 0.87H_2O$, or simplified as $C \cdot S \cdot H_{0.87}$. Thus, the theoretically maximum mass increase W_{max} should be 33.4% in view of Eqs. (5) and (6).
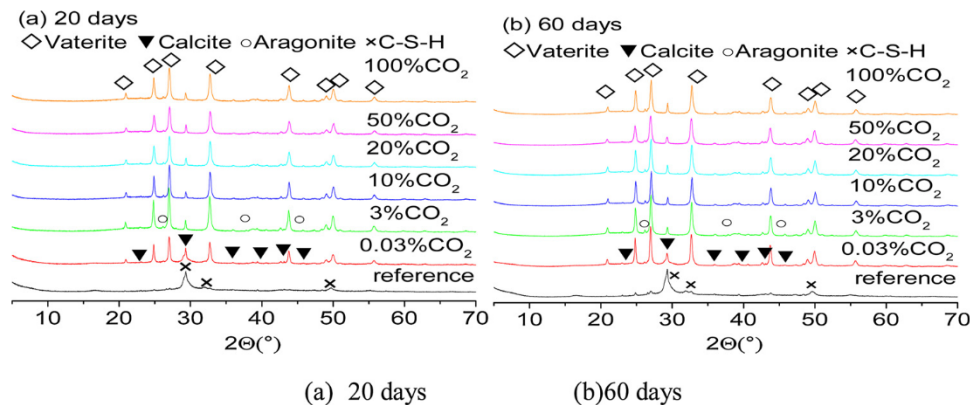
(a) 20 days   (b)60 days

Fig. 6. Diffractograms of C-S-H under carbonation at different conditions for 20 days (a) and 60 days (b).
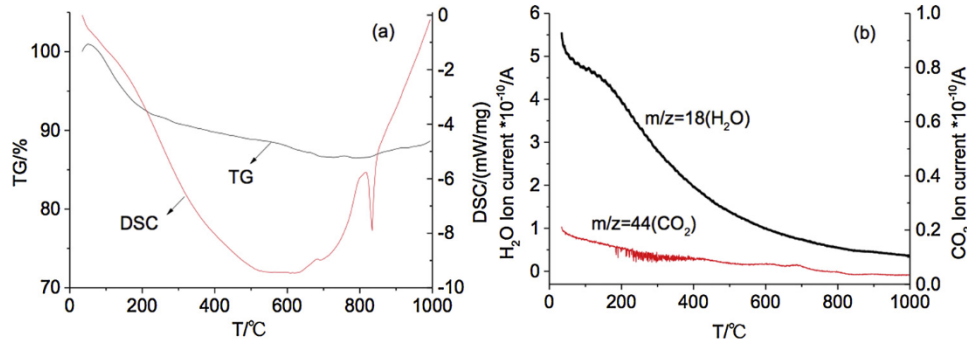
Fig. 7. TG/DSC (a) coupled with mass spectrometer (MS, (b)) performed on uncarbonated sample.
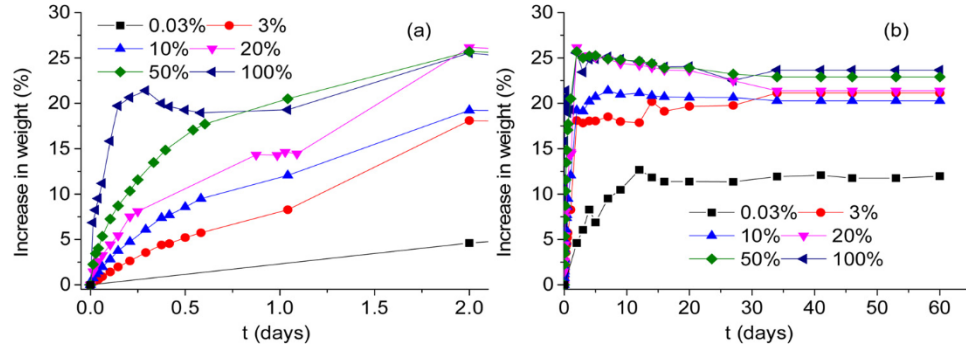

Fig. 8. Mass increase of samples in wt% under different concentration of CO$_2$ after 2 (a) and 60 (b) days.

3.3.2. Carbonation kinetics under different CO$_2$ concentrations

The evolution of the samples' mass increase under different carbonation conditions are shown in Fig. 8. The mass increasing rate increased with higher CO$_2$ concentration. There was no further mass increase in the accelerated and natural conditions after carbonation of 2 and 20 days, respectively. The carbonation reaction could be divided into two stages: for stage-1, the sample mass increased continuously with the prolonging of exposure time; for stage-2, the sample mass was almost stable and even showed a slight decrease, because of water dissipation. In general, no further mass increase for all the samples after 20 days was observed, indicating the completion of the carbonation process.

Here, the carbonation degree for the synthetic C-S-H was calculated according to Eq. (7), as follows:
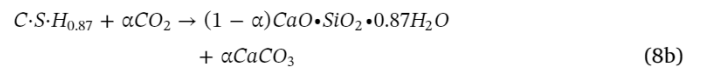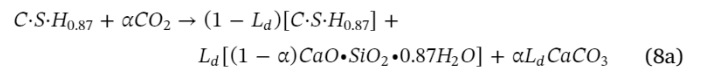
$$\alpha = \frac{W(t)}{W_{max}} \tag{7}$$

where $W(t)$ represents the mass increase at time t and W_{max} denotes the theoretical maximum mass increase, which was determined by TGA-MS analysis in Section 3.3.1 as 33.4%.

Morandeau et al. [6] suggested that carbonation of C-S-H will not release any physical water, which means the water produced from C-S-H carbonation will be absorbed by the silica gel. That is also verified by Thiery et al. [49] by saying that characteristic times of carbonation and drying are sufficiently separated in carbonation process. Therefore, in this study, the mass increase in stage-1 was resulted from the reaction with CO$_2$ so that the mass change at this stage can reflect the carbonation degree based on Eq. (7). However, samples' mass showed decreasing tendency at stage-2, which is attributed to effect of drying at surrounding RH of 72%. The carbonation degree at stage-2 converted from mass change was, therefore, somehow underestimated compared with the true value. Therefore, the analysis of carbonation kinetics in this study are relied on the data from stage-1.

Fig. 9 indicates the carbonation degree of C-S-H at different accelerated conditions. It can be seen from Fig. 9 that the carbonation degree of C-S-H was lower than 0.8 under all carbonation conditions. In

view of the NMR results, some of C-S-H was still remained, especially when carbonated at atmospheric environment (0.03% CO$_2$), which was disappeared under the accelerating carbonation. Thus, two equations, written as Eq. (8a) and (8b). were used to describe the carbonation reaction of C-S-H in 0.03% CO$_2$ and accelerating carbonation. For C-S-H carbonated under natural condition, only part of C-S-H was decalcified to form as the mixture of uncarbonated C-S-H, calcium carbonate and decalcified C-S-H (calcium modified silica gel and silica gel), as expressed by Eq. (8a). However, for the sample carbonated under accelerated conditions, calcium carbonate and decalcified C-S-H (calcium modified silica gel and silica gel) coexisted together, as expressed by Eq. (8b), respectively.

$$C \cdot S \cdot H_{0.87} + \alpha CO_2 \rightarrow (1 - L_d)[C \cdot S \cdot H_{0.87}] +$$
$$L_d[(1 - \alpha)CaO \bullet SiO_2 \bullet 0.87H_2O] + \alpha L_d CaCO_3 \tag{8a}$$

$$C \cdot S \cdot H_{0.87} + \alpha CO_2 \rightarrow (1 - \alpha)CaO \bullet SiO_2 \bullet 0.87H_2O$$
$$+ \alpha CaCO_3 \tag{8b}$$

In the review of [21,50–53], the carbonation kinetics can be expressed by Eq. (9),

$$[1 - (1 - \alpha)^{1/3}]^n = kt \tag{9}$$

where k is a constant value of reaction rate, t is the carbonation time (h), and n is a factor indicating the different steps during carbonation. The reaction rate constant k is determined by the logarithmic form, and Eq. (9) to can be rewritten as Eq. (10).

$$\ln[1 - (1 - \alpha)^{1/3}] = \frac{1}{n}\ln(k) + \frac{1}{n}\ln(t) \tag{10}$$

Fig. 10 gives the tested data fitted with the model, represented by Eq. (9) and Eq. (10). Two stages were fitted for any kind of conditions, and only fitting parameters of stage-1 were given in Table 5, which represented the reaction rate of carbonation. When the slope of the model ($1/n$) equals to 1, Eq. (9) was defined as the "contracting volume" equation, which implies that the carbonation is controlled by the phase boundary [50,51]. For $1/n = 0.5$, Eq. (9) was represented as the
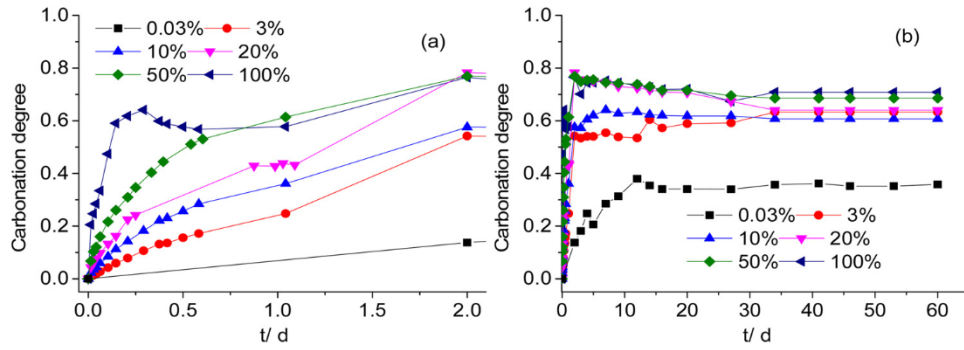
Fig. 9. Carbonation degree of synthetic C-S-H under different concentration of CO_2 after 2 (a) and 60 (b) days.
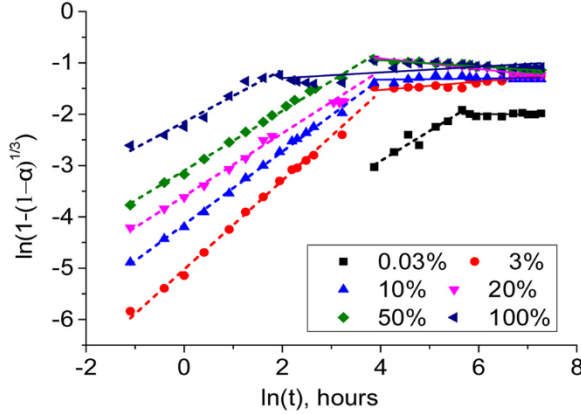

Fig. 10. Plots representing the model-predicted (lines) and actual (data points) value of $\ln(1 - (1 - \alpha)^{1/3})$ vs. $\ln(t)$ for carbonation kinetics of different concentration of CO_2. Dashed line and solid line represent stage-1 and stage-2 of carbonation reaction, respectively.

Table 5
Fitting parameters of carbonation kinetic model of different CO_2 concentrations.

Sample	Slope (1/n)	Intercept(ln(k)/n)	$k/(10^{-4}\,h^{-1})$
0.03%CO₂	0.58	−6.25	0.21
3%CO₂	0.87	−5.02	29.17
10%CO₂	0.71	−4.14	29.23
20%CO₂	0.61	−3.50	32.73
50%CO₂	0.58	−3.10	47.73
100%CO₂	0.51	−2.15	147.62

Jander's equation, which suggests that layer forms of reaction products were coated outside the uniform size of reactants so that reaction rate was affected by the diffusion rate through the outer-layer [50–52]. Other studies have proved the evolution of the phase-boundary controlled to diffusion controlled stages during the carbonation process [21,53]. However, in this study, only one kind of reaction was found in Fig. 10. In actual experiment, to keep the concentration steady, the mass changes were recorded after 20 min of carbonation. It is assumed that the phase-boundary controlled reaction has been finished in the first 20 min. After then, the diffusion controlled stage became dominant. Therefore, the mass changes recorded in this study should follow the diffusion controlled reaction, which means the ideal slope of $1/n$ should be equal to 0.5. As shown in Table 5, the slope of the fitting curves were varying form 0.51 to 0.87. The fitted slope ($1/n$) for 100% CO_2 carbonated sample (0.51) was very close to 0.5. For other samples, the fitted slope ($1/n$) ranged from 0.58 to 0.87. Such difference between the calculated and theoretical values was also observed by Ashraf [21]. It was because that carbonation process is more complicated in practice. In summary, Eq. (9) provided a simplified model for carbonation

kinetics.

3.3.3. Effect of different CO_2 concentrations on the carbonation rate

Table 5 shows that the reaction rate constant k increased rapidly when CO_2 concentration (C_{CO_2}) was higher than 20%, and reached the fastest rate ($147.62 \times 10^{-4}\,h^{-1}$) under 100% CO_2, suggesting the similar reaction kinetics between 3% and 20% CO_2. The Boltzmann function in Eq. (11) was used to fit the relationship between the reaction rate constant (k) and CO_2 concentration under accelerated carbonation, as shown in Fig. 11. However, the carbonation rate constant under natural carbonation (0.03% CO_2) was much smaller than that under the accelerated conditions. Herein, the CO_2 concentration between 0.03% and 3% was not studied, and the reaction rate constant in this range remained unknown. The dashed line was used to describe the relation from 0.03% to 3% CO_2.

$$k = 679.68 - 655.2/$$
$$(1 + exp((C_{CO_2} - 139.8)/27.19)),$$
$$3 \leq x \leq 100, \; R^2 = 0.99 \tag{11}$$

4. Discussion

4.1. Crystal precipitation of allotropic forms of calcium carbonate after carbonation

As reported in the literatures, the carbonation of portlandite and C-S-H under ambient environment follows the initial formation of amorphous calcium carbonate (ACC) which is then transformed to metastable forms of vaterite and aragonite, and finally calcite is formed through dissolution-precipitation process [54–56]. However, Our investigation shows that vaterite is the dominant phase after carbonation of pure C-S-H, which is different from the carbonation of cement paste that calcite and vaterite are the main products [30,38]. The difference in carbonation products between pure C-S-H and cement paste could be ascribed to the following reasons.
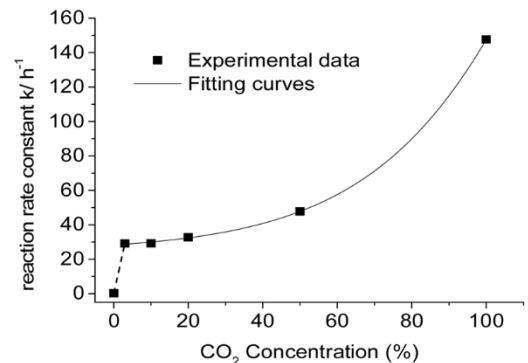

Fig. 11. Experimental and fitted data of reaction rate constant of carbonation.

Firstly, the pH value of pore solution in cement paste is at least 12.5 [57–59]. Calcite is the only stable form for allotropic calcium carbonate [60] and supersaturated rapidly in such solution with high alkalinity [61,62]. Thus, once carbonation occurs, calcite will be precipitated with the consumptions of Ca^{2+} and OH^- in pore solution. However, there is high content of solid portlandite in the cement paste, which will dissolve into solution to compensate the consumptions of Ca^{2+} and OH^- and to keep the pH at its high level. When carbonation proceeds and portlandite is completely consumed, the pH of pore solution will be decreased to lower than 9 [57,58]. It is the value that precipitation of vaterite become predominant [27,60]. This could explain the coexistence of calcite and vaterite after the carbonation of cement paste [30,38].

However, for the pure C-S-H in this study, with initial pH at around 11.5 [41,63], the pH will be decreased immediately when carbonation starts. Hence, the predominant precipitation of vaterite is expected due to the low pH value after carbonation [57,58]. The transformation of vaterite to calcite is possible but its rate is very limited, as verified by the data in Tables 3 and 4. The low transformation rate can also be attributed to the lack of water (72% RH) [27]. In addition, the preferable precipitation of calcium carbonate is also affected by the properties of C-S-H. It is suggested that C-S-H we used in this research (Ca/Si = 1) has a calcium octahedral sheets structure, similar symmetries, and a positive surface charge to form as vaterite [64], while C-S-H with higher Ca/Si ratio may have structures similar to both vaterite and calcite [18].

Furthermore, the presence of aragonite for both cement paste and C-S-H carbonation could be ascribed to the formation of amorphous calcium modified silica gel after carbonation [64].

4.2. Carbonation and decalcification degree of C-S-H under different CO₂ concentrations

The carbonation degree defined in this paper is referred to the "proportion of calcium precipitating as calcium carbonate". After carbonation, calcium will be contained in the residue C-S-H, decalcified C-S-H and calcium carbonate. However, the decalcification degree is determined only by the remaining proportion of Q_1, Q_{2b} and Q_{2p}, deconvolved from the NMR results. From Table 2 and Fig. 9, even though the decalcification degree under the accelerated carbonation was close to 100%, the carbonation degree for all samples are below 0.8. It means that apart from the residue C-S-H, decalcified C-S-H also contained calcium. One should note that definition of carbonation degree by Eq. (7) is different from that of decalcification degree (also as decalcification level) by Eq. (2) in this paper.

The carbonation degree for all samples cannot reach the ideal value 1.0, which is mainly triggered by the blocking of calcium carbonate at the gel pore to prevent the total decalcification of C-S-H. After 60 days carbonation, the degree of carbonation in the sample carbonated under natural environment was always much lower than that under the accelerated carbonation conditions. It has been observed that the carbonation degrees under 3% to 20% CO₂ are similar, but lower than that under 50% and 100% CO₂. This is consistent with the kinetics analysis in Section 3.3.3, that is, the carbonation effects from 3% to 20% CO₂ are similar. Therefore, from the view of carbonation degree and kinetics, 20% CO₂ is advised to use for the accelerated carbonation, which has the highest rate but shows little influence on the final carbonation degree and kinetics.

Moreover, when C-S-H was mixed with other hydration productions, such as portlandite and AFm, to form as cement paste, the decalcification degree of C-S-H after carbonation was different from synthetic C-S-H powder. Auroy et al. [30] have found that decalcification degrees induced by carbonation for cement paste varying from 76% to 92%. A former study conducted by the authors also proved that the decalcification degree of C-S-H in cement paste was about 80% [38]. However, in this research, the value of decalcification degree increased

to 100% for pure C-S-H under accelerated carbonation. It is because of the difference in the carbonation kinetics between the cement paste and synthetic C-S-H. For a hydrated cement mixture, CO₂ diffuses through both capillary and gel pores, and then dissolves into the pore solution to react with the calcium ions from the pore solution. The way that CO₂ diffuses into cement mixture should follow the Fick's second law, so that CO₂ distribution in the cement follow the decreasing gradient. However, CO₂ can dissolve directly into the gel pores at the synthetic C-S-H surface. This difference of reaction kinetics may affect the final decalcification degree. In addition, after the carbonation of cement paste, pores will be blocked by the formation of calcium carbonate. The portlandite has a size around 3–5 μm [65], whose volume will expand further when it is carbonated to form as calcium carbonate. The porosity of cement paste will decrease considerable after carbonation. Therefore, the big size of the carbonated portlandite will not only hinder the decalcification of C-S-H located behind the portlandite, but also protect the inner C-S-H from the decalcification due to lower diffusion rate of CO₂, while no portlandite hinders the further decalcification of pure C-S-H. The NMR results, displayed in Tables 1 and 2, presented that the decalcification degree of synthetic C-S-H in all CO₂ concentrations were similar that C-S-H was completely decalcified after the accelerated carbonation. As a result, it is believed that the decalcification process of synthetic C-S-H is not affected by the CO₂ concentration, but the decalcification degree of C-S-H in cement paste is related to carbonation kinetics and the existence of portlandite. Our former study has also verified that the CO₂ concentration below 20% would not change the decalcification degree dramatically for the cement paste [38].

4.3. Concerns of durability and sustainability of concrete with natural and accelerated carbonation

The results we got above are beneficial for evaluating both durability and sustainability properties of concrete structures under carbonation. Investigation has been conducted to evaluate the feasibility for storage of natural CO₂ in concrete due to carbonation [66–70]. It is shown in this study that C-S-H is difficult to be fully carbonated under the natural condition (only approximately 40% according to Eq. 8a). The carbonation products consisted of residue C-S-H, calcium carbonate and decalcified C-S-H. Former study also verified the low decalcification degree of C-S-H in cement paste after natural carbonation [38]. Thus, the potential of CO₂ storage in concrete has not been fully exploited under natural condition. Actually, the CO₂ storage capacity of concrete can be improved twice if full carbonation is considered. More details about improving CO₂ storage capacity of concrete should be further studied.

Moreover, the carbonation performance of cement-based materials nowadays are often obtained via accelerated carbonation, which is totally different to that under natural carbonation, even under 3% CO₂, in view of the results above. Though the relationship of carbonation depths between natural and accelerated conditions has been reported by some researchers [32,71,72], the differences in chemical phases and reaction kinetics between natural and accelerated carbonations are rarely considered, which actually is quite different on the basis of the data in this paper. The carbonation results gotten from accelerated conditions should be considered carefully before used for predicting the carbonation performance of concrete under natural condition.

Another sustainability issue of CO₂ concerning recycled aggregate concrete (RAC) should also be considered. Thanks to the development of industry and economy, the generation of construction and demolition waste (C&DW) in daily life has brought heavy burden on the earth environment [73–75]. Producing RAC by recycled aggregates has been seen as a valid method for reutilization of C&DW [76–78]. However, due to its high water sorption, high porosity and low mechanical properties, the durability properties of RAC is more inferior compared to the concrete made of natural aggregates [79,80]. The accelerated

carbonation has been adopted to pre-carbonate the recycled concrete aggregate (RCA) to get better quality and mechanical properties of RAC [81,82]. Based on the data mentioned above, the decalcification degree of C-S-H is similar under accelerated conditions and higher than that under natural condition. Though the carbonation kinetics below 20% CO_2 is the same and different from those conditions higher than 20% CO_2 (as shown in Table 5), the decalcification results of C-S-H and compositions of allotropic calcium carbonates are not affected by the CO_2 concentration. It is advised to use higher concentration of CO_2 to pre-carbonate the RCA in order to get higher rate and degree of carbonation.

5. Conclusion

In this study, the synthetic C-S-H with Ca/Si = 1.0 was carbonated under natural and accelerated conditions using different concentrations of CO_2. The SEM and TEM were used for microstructure characterisation. The ^{29}Si MAS-NMR, XRD and TGA-MS methods were applied for the quantitative and qualitative analysis of chemical phases after carbonation. The carbonation kinetics were analysed for explaining the carbonation rate under different CO_2 concentrations.

The data from NMR measurements showed that C-S-H will be decalcified partly under natural condition and completely under accelerated conditions. With the increase in carbonation duration, the degree of polymerisation will be improved further by a slow rate. The compositions of decalcified C-S-H were not affected by the concentration of CO_2.

Quantitative XRD analysis suggested that three allotropic forms of calcium carbonate, i.e. vaterite, aragonite and calcite were formed after carbonation, with the dominant proportion of vaterite. More aragonite and calcite will be transformed from vaterite for further carbonation. The preferred formation of calcium carbonate was not influenced by the CO_2 concentration under accelerated carbonation conditions.

The stoichiometric formula of synthetic C-S-H was $CaO \bullet SiO_2 \bullet 0.87 H_2O$ or $C \cdot S \cdot H_{0.87}$. The carbonation reaction proceeded differently under natural and accelerated conditions. Two equations (8(a) and 8(b)) were used to describe the chemical reactions under natural and accelerated carbonations, respectively.

The carbonation kinetics of C-S-H under different CO_2 concentrations were studied, and the experimental data fitted well with the employed model. The carbonation rate constant kept almost similar, when CO_2 concentration was in a range of 3–20%, and increased dramatically when CO_2 concentration was higher than 20%. The carbonation kinetics between 3% and 20% CO_2 are similar, but different from that under 50% and 100% CO_2.

The decalcification results of pure synthetic C-S-H are not affected by the CO_2 concentration and 100% decalcification degree is reached under accelerated carbonation. However, the final carbonation degree of C-S-H will be impacted by the carbonation concentration.

Declaration of Competing Interest

The authors have declared that there is no conflict of interest regarding the publication of this research article.

Acknowledgement

References

[1] S.O. Ekolu, A review on effects of curing, sheltering, and CO_2 concentration upon natural carbonation of concrete, Constr. Build. Mater. 127 (2016) 306–320.

[2] M.F. Ba, T. Xue, Z.M. He, et al., Carbonation of magnesium oxysulfate cement and its influence on mechanical performance, Constr. Build. Mater. 223 (2019) 1030–1037.

[3] H. El-Hassan, Y. Shao, Carbon storage through concrete block carbonation, J. Clean. Energy. Technol. 2 (2014) 287–291.

[4] T.F. Sevelsted, J. Skibsted, Carbonation of C–S–H and C–A–S–H samples studied by ^{13}C, ^{27}Al and ^{29}Si MAS NMR spectroscopy, Cem. Concr. Res. 71 (2015) 56–65.

[5] C. Alonso, C. Andrade, J.A. González, Relation between resistivity and corrosion rate of reinforcements in carbonated mortar made with several cement types, Cem. Concr. Res. 18 (1988) 687–698.

[6] A. Morandeau, M. Thiéry, P. Dangla, Investigation of the carbonation mechanism of CH and C-S-H in terms of kinetics, microstructure changes and moisture properties, Cem. Concr. Res. 56 (2014) 153–170.

[7] X. Cong, R.J. Kirkpatrick, ^{29}Si MAS NMR study of the structure of calcium silicate hydrate, Adv. Cem. Based Mater. 3 (1996) 144–156.

[8] A.R. Brough, C.M. DobsonIan, Application of selective ^{29}Si isotopic enrichment to studies of the structure of calcium silicate hydrate (C–S–H) gels, J. Am. Ceram. Soc. 77 (1994) 593–596.

[9] I. Klur, B. Pollet, J. Virlet, C-S-H Structure Evolution With Calcium Content by Multinuclear NMR, Springer, Berlin, 1998.

[10] K. Kobayashi, K. Suzuki, Y. Uno, Carbonation of concrete structures and decomposition of C-S-H, Cem. Concr. Res. 24 (1994) 55–61.

[11] H.F.W. Taylor, Proposed structure for calcium silicate hydrate gel, J. Am, Ceram. Soc. 69 (1986) 464–467.

[12] H.F.W. Taylor, Nanostructure of C-S-H: current status, Adv. Cem. Based Mater. 1 (1993) 38–46.

[13] I.G. Richardson, The calcium silicate hydrates, Cem. Concr. Res. 38 (2008) 137–158.

[14] V. Morales-Florez, N. Findling, F. Brunet, Changes on the nanostructure of cementitius calcium silicate hydrates (C–S–H) induced by aqueous carbonation, J. Mater. Sci. 47 (2011) 764–771.

[15] B. Lothenbach, K. Scrivener, R.D. Hooton, Supplementary cementitious materials, Cem. Concr. Res. 41 (2011) 1244–1256.

[16] I.G. Richardson, The nature of C-S-H in hardened cements, Cem. Concr. Res. 29 (1999) 1131–1147.

[17] R. Taylor, I.G. Richardson, R.M.D. Brydson, Nature of C–S–H in 20 year old neat ordinary Portland cement and 10% Portland cement–90% ground granulated blast furnace slag pastes, Adv. Appl. Ceram. 106 (2013) 294–301.

[18] J. Li, Q. Yu, H. Huang, et al., Effects of Ca/Si ratio, aluminum and magnesium on the carbonation behavior of calcium silicate hydrate, Materials 12 (2019) 2–14.

[19] W. Ashraf, J. Olek, Elucidating the accelerated carbonation products of calcium silicates using multi-technique approach, J. CO2 Util. 23 (2018) 61–74.

[20] M. Castellote, L. Fernandez, C. Andrade, et al., Chemical changes and phase analysis of OPC pastes carbonated at different CO_2 concentrations, Mater. Struct. 42 (2008) 515–525.

[21] W. Ashraf, J. Olek, Carbonation activated binders from pure calcium silicates: reaction kinetics and performance controlling factors, Cem. Concr. Compos. 93 (2018) 85–98.

[22] G. Villain, M. Thiery, G. Platret, Measurement methods of carbonation profiles in concrete: Thermogravimetry, chemical analysis and gammadensimetry, Cem. Concr. Res. 37 (2007) 1182–1192.

[23] S. Goni, M.T. Gaztañaga, A. Guerrero, Role of cement type on carbonation attack, J. Mater. Res. 17 (2002) 1834–1842.

[24] A. Hidalgo, C. Domingo, C. Garcia, et al., Microstructural changes induced in Portland cement-based materials due to natural and supercritical carbonation, J. Mater. Sci. 43 (2008) 3101–3111.

[25] M. Thiery, G. Villain, P. Dangla, et al., Investigation of the carbonation front shape on cementitious materials: effects of the chemical kinetics, Cem. Concr. Res. 37 (2007) 1047–1058.

[26] M. Kitamura, Strategy for control of crystallization of polymorphs, CrystEngComm 11 (2009) 949–964.

[27] Y.S. Han, G.W. Hadiko, M. Fuji, et al., Crystallization and transformation of vaterite at controlled pH, J. Cryst. Growth 289 (2006) 269–274.

[28] H. Deng, S. Wang, X. Wang, et al., Two competitive nucleation mechanisms of calcium carbonate biomineralization in response to surface functionality in low calcium ion concentration solution, Regen. Biomater. 2 (2015) 187–195.

[29] W. Ashraf, Carbonation of cement-based materials: challenges and opportunities, Constr. Build. Mater. 120 (2016) 558–570.

[30] M. Auroy, S. Poyet, P.L. Bescop, et al., Comparison between natural and accelerated carbonation (3% CO_2): impact on mineralogy, microstructure, water retention and cracking, Cem. Concr. Res. 109 (2018) 64–80.

[31] E. Drouet, S. Poyet, P. Le Bescop, et al., Carbonation of hardened cement pastes: influence of temperature, Cem. Concr. Res. 115 (2019) 445–459.

[32] H.Z. Cui, W.C. Tang, W. Liu, et al., Experimental study on effects of CO_2 concentrations on concrete carbonation and diffusion mechanisms, Constr. Build. Mater. 93 (2015) 522–527.

[33] NORDTEST, Concrete, Repairing Materials and Protective Coating Carbonation Resistance, NT BUILD 357, Finland, 1989.

[34] GB/T50082-2009, Standard for Test Methods of Long-term Performance and Durability of Ordinary Concrete, Ministry of Housing and Urban-Rural Development of the People's Republic of China, Beijing, 2009.

[35] T.A. Harrison, M.R. Jones, M.D. Newlands, et al., Experience of using the prTS 12390-12 accelerated carbonation test to assess the relative performance of concrete, Mag. Concrete. Res. 64 (2012) 737–747.

[36] D. Zhang, Z. Ghouleh, Y.X. Shao, Review on carbonation curing of cement-based materials, J. CO2 Util. 21 (2017) 119–131.

[37] S.P. Wang, X.Q. Peng, L.P. Tang, et al., Influence of hydrothermal synthesis conditions on the formation of calcium silicate hydrates: from amorphous to crystalline

phases, J. Wuhan Univ. Technol. 33 (2018) 1151–1158.

[38] W. Liu, Y.Q. Li, L.P. Tang, et al., XRD and ^{29}Si MAS NMR study on carbonated cement paste under accelerated carbonation using different concentration of CO_2, Mater. Today. Commun. 19 (2019) 464–470.

[39] A.J. Vega, G.W. Scherer, Study of structural evolution of silica gel using ^{1}H and ^{29}Si NMR, J. Non-Cryst. Solids. 111 (1989) 153–166.

[40] Y. Okada, ^{29}Si NMR spectroscopy of silicate anions in hydrothermally formed C–S–H, J. Am. Ceram. Soc. 77 (1994) 765–768.

[41] J.J. Chen, J.J. Thomas, H.F.W. Taylor, et al., Solubility and structure of calcium silicate hydrate, Cem. Concr. Res. 34 (2004) 1499–1519.

[42] R.J. Myers, S.A. Bernal, J.D. Gehman, et al., The role of Al in cross-linking of alkali-activated slag cements, J. Am. Ceram. Soc. 98 (2015) 996–1004.

[43] I.G. Richardson, J. Skibsted, L. Black, et al., Characterisation of cement hydrate phases by TEM, NMR and Raman spectroscopy, Adv. Cem. Res. 22 (2010) 233–248.

[44] M. Grutzeck, A. Benesi, B. Fanning, Silicon-29 magic angle spinning nuclear magnetic resonance study of calcium silicate hydrates, J. Am. Ceram. Soc. 72 (1989) 665–668.

[45] D. Wang, Y.F. Fang, Y.Y. Zhang, et al., Changes in mineral composition, growth of calcite crystal, and promotion of physico-chemical properties induced by carbonation of β-C2S, J. CO2 Util. 34 (2019) 149–162.

[46] L. Fernández-Díaz, Á. Fernández-González, M. Prieto, The role of sulfate groups in controlling $CaCO_3$ polymorphism, Geochim. Cosmochim. Ac. 74 (2010) 6064–6076.

[47] T.S.T. Ogino, K. Sawada, The formation and transformation mechanism of calcium carbonate in water, Geochim. Cosmochim. Ac. 51 (1987) 2757–2767.

[48] J. Chang, Y.F. Fang, Quantitative analysis of accelerated carbonation products of the synthetic calcium silicate hydrate(C–S–H) by QXRD and TG/MS, J. Therm. Anal. Calorim. 119 (2014) 57–62.

[49] M. Thiery, P. Dangla, P. Belin, et al., Carbonation kinetics of a bed of recycled concrete aggregates: a laboratory study on model materials, Cem. Concr. Res. 46 (2013) 50–65.

[50] M. Brown, D. Dollimore, A. Galwey, Theory of solid state reaction kinetics, Compr. Chem. Kinet. 22 (1980) 41–113.

[51] A. Khawam, D.R. Flanagan, Solid-state kinetic models basics and mathematical fundamentals, J. Phys. Chem. B 110 (2006) 17315–17328.

[52] E.A. Giess, Equations and tables for analyzing solid-state reaction kinetics, J. Am. Ceram. Soc. 43 (1963) 374–376.

[53] J. Sun, M.F. Bertos, S.J.R. Simons, Kinetic study of accelerated carbonation of municipal solid waste incinerator air pollution control residues for sequestration of flue gas CO_2, Energ. Environ. Sci. 1 (2008) 370–377.

[54] C. Rodriguez-Navarro, K. Elert, R. Ševčík, Amorphous and crystalline calcium carbonate phases during carbonation of nanolimes: Implications in heritage conservation, CrystEngComm 18 (2016) 6594–6607.

[55] D.T. Beruto, R. Botter, Liquid-like H_2O adsorption layers to catalyze the $Ca(OH)_2$/CO_2 solid-gas reaction and to form a non-protective solid product layer at 20 °C, J. Eur. Ceram. Soc. 20 (2000) 497–503.

[56] R. Camerini, G. Poggi, D. Chelazzi, et al., The carbonation kinetics of calcium hydroxide nanoparticles: a boundary nucleation and growth description, J. Colloid Interface Sci. 547 (2019) 370–381.

[57] J. Chang, D. Wang, Y.F. Fang, Effects of mineralogical changes in BOFS during carbonation on pH and Ca and Si leaching, Constr. Build. Mater. 192 (2018) 584–592.

[58] X.M. Wan, F.H. Wittmann, T.J. Zhao, et al., Chloride content and pH value in the pore solution of concrete under carbonation, J. Zhejiang. Univ-Sc. A. 14 (2013) 71–78.

[59] G. Plusquellec, M.R. Geiker, J. Lindgård, et al., Determination of the pH and the free alkali metal content in the pore solution of concrete: review and experimental comparison, Cem. Concr. Res. 96 (2017) 13–26.

[60] Ç. Oral, B. Ercan, Influence of pH on morphology, size and polymorph of room temperature synthesized calcium carbonate particles, Powder Technol. 339 (2018) 781–788.

[61] J. Gomez-Morales, J. Torrent-Burgues, R. Rodrfguez-Clemente, Nucleation of calcium carbonate at different initial pH conditions, J. Cryst. Growth 169 (1996) 331–338.

[62] W.S. Kim, I. Hirasawa, W.S. Kim, Polymorphic change of calcium carbonate during reaction crystallization in a batch reactor, Ind. Eng. Chem. Res. 43 (2004) 2650–2657.

[63] C.S. Walker, D. Savage, M. Tyrer, et al., Non-ideal solid solution aqueous solution modeling of synthetic calcium silicate hydrate, Cem. Concr. Res. 37 (2007) 502–511.

[64] L. Black, C. Breen, J. Yarwood, et al., Structural features of C-S-H(I) and its carbonation in air—a Raman spectroscopic study. Part II: carbonated phases, J. Am. Ceram. Soc. 90 (2007) 908–917.

[65] L. Qin, X.J. Gao, Properties of coal gangue-Portland cement mixture with carbonation, Fuel 245 (2019) 1–12.

[66] A. Dindi, D.V. Quang, L.F. Vega, et al., Applications of fly ash for CO_2 capture, utilization, and storage, J. CO2 Util. 29 (2019) 82–102.

[67] R.M. Cuéllar-Franca, A. Azapagic, Carbon capture, storage and utilisation technologies: A critical analysis and comparison of their life cycle environmental impacts, J. CO2 Util. 9 (2015) 82–102.

[68] R. Kurda, J. de Brito, J.D. Silvestre, Carbonation of concrete made with high amount of fly ash and recycled concrete aggregates for utilization of CO_2, J. CO2 Util. 29 (2019) 12–19.

[69] M.N. Anwar, A. Fayyaz, N.F. Sohail, et al., CO_2capture and storage: A way forward for sustainable environment, J. Environ. Manage. 226 (2018) 131–144.

[70] J.D. Filippo, J. Karpman, J.R. DeShazo, The impacts of policies to reduce CO_2 emissions within the concrete supply chain, Cem. Concr. Compos. 101 (2019) 67–82.

[71] V.G. Papadakis, C.G. Vayenas, Experimental investigation and mathematical modeling of the concrete carbonation problem, Chem. Eng. Sci. 46 (1991) 1333–1338.

[72] X.Y. Wang, H.S. Lee, A model predicting carbonation depth of concrete containing silica fume, Mater. Struct. 42 (2008) 691–704.

[73] F. Martirena, T. Castano, A. Alujas, et al., Improving quality of coarse recycled aggregates through cement coating, J. S. Cem. Mater. 6 (2017) 69–84.

[74] R.V. Silva, J. Brito, R.K. Dhir, Properties and composition of recycled aggregates from construction and demolition waste suitable for concrete production, Constr. Build. Mater. 65 (2014) 201–217.

[75] V. Babu, A. Mullick, K. Jain, et al., Strength and durability characteristics of high-strength concrete with recycled aggregate-influence of processing, J. S. Cem. Mater. 4 (2015) 44–53.

[76] D.X. Xuan, B.J. Zhan, C.S. Poon, Assessment of mechanical properties of concrete incorporating carbonated recycled concrete aggregates, Cem. Concr. Compos. 65 (2016) 67–74.

[77] J.K. Zhang, C.J. Shi, Y.K. Li, et al., Performance enhancement of recycled concrete aggregates through carbonation, J. Mater Civ. Eng. 27 (2015) 04015029.

[78] V.W. Tam, A. Butera, K.N. Le, Carbon-conditioned recycled aggregate in concrete production, J. Clean. Prod. 133 (2016) 672–680.

[79] J.Z. Xiao, D. Lu, J.W. Ying, Durability of recycled aggregate concrete: an overview, J. Adv. Concr. Technol. 11 (2013) 347–359.

[80] S.C. Kou, C.S. Poon, Enhancing the durability properties of concrete prepared with coarse recycled aggregate, Constr. Build. Mater. 35 (2012) 69–76.

[81] C.J. Shi, F.Q. He, Y.Z. Wu, Effect of pre-conditioning on CO_2 curing of lightweight concrete blocks mixtures, Constr. Build. Mater. 26 (2012) 257–267.

[82] C.J. Shi, D.H. Wang, F.Q. He, et al., Weathering properties of CO_2-cured concrete blocks, Resour. Conserv. Recycl. 65 (2012) 11–17.